Title
Dynamics of human neocortex that optimizes its stability and flexibility

Journal
INTERNATIONAL JOURNAL OF INTELLIGENT SYSTEMS, 21(9)

ISSN
0884-8173

Authors
Freeman, Walter J, III
Holmes, M D
West, G A
et al.

Publication Date
2006-09-01

Peer reviewed

Dynamics of human neocortex that optimizes its stability and flexibility

International Journal of Intelligent Systems 21: 881-901, 2006

Walter J Freeman[1], Mark D Holmes[2], G Alexander West[3], Sampsa Vanhatalo[4]

[1]Department of Molecular & Cell Biology
University of California at Berkeley
Berkeley CA 94720-3200 USA
Tel: 510-642-4220 fax: 510-643-6791
wfreeman@socrates.berkeley.edu

[2]EEG & Clinical Neurophysiology Laboratory
Department of Neurology
University of Washington
325 Ninth Ave, Harborview Medical Center
Box 359722, Seattle, WA 98104
tel: 206-731-3539 fax: 206-731-4409
mdholmes@u.washington.edu

[3]Department of Neurological Surgery
University of Washington
Box 359766 Seattle, WA 98104
tel: 206-521-1848 fax: 206-521-1881
gaw@u.washington.edu

[4]Department of Clinical Neurophysiology
University of Helsinki
Helsinki, Finland
sampsa.vanhatalo@helsinki.fi

Running title: Stability and flexibility of human neocortex

Key Words: EEG intracranial, power-law distributions, Hilbert transform, neurodynamics, phase cone, phase gradient, self-organized criticality (SOC)

Acknowledgments

The human data were collected in the EEG & Clinical Neurophysiology Laboratory, Harborview Medical Center, Seattle WA. The 8x8 electrode array was constructed by Ad-Tech Medical Instrument Corp. Racine WI 53404 in accordance with a Berkeley design. Programming was by Brian C. Burke in the Division of Neurobiology at Berkeley. Partial support was provided through grants NCC 2-1244 from NASA and EIA-0130352 from NSF to Robert Kozma. We are grateful for support from Dr. Scott Barnhart, Medical Director, Harborview Medical Center, Seattle WA.

Abstract

The electroencephalogram (EEG) in normal resting subjects is robustly stable. In epileptic subjects it reveals instability. We investigated EEGs in states of a neurosurgical patient awake and at rest, in sleep, and in intractable partial complex seizures. We used a microgrid array of 64 electrodes in a 1x1 cm window fixed on the right inferior temporal gyrus. EEG signals were recorded during a week of neurosurgical evaluation for treatment. Comparisons with normal intracranial EEG were perforce made with data from animal studies. Analytic phase and amplitude were calculated with the Hilbert transform to get the temporal resolution needed to reveal spatiotemporal structure in the background EEG, The rest state revealed multiple overlapping patterns of local coherent oscillations in the beta range with conic phase gradients that had the appearance of bubbles in a pan of boiling water or droplets condensing and evaporating in fog. Cone diameters gave estimates of the distances across cortex over which the cortical oscillations were synchronized. Superimposed on shorter and smaller phase cones were larger and longer epochs of phase locking with briefly near-constant frequency and high amplitude. These coordinated analytic phase differences (CAPD) occurred between short periods of high spatial variance in phase differences. We interpreted the variance as evidence for phase transitions between transiently stable states, each demarcated by a stable phase cone. In sleep the phase cones and CAPD persisted with reduced amplitude, occasionally interrupted by long-lasting (~1 s) epochs with no spatial textures in phase and amplitude despite large increases in amplitude. A local seizure consisted of high amplitude 3/s waves with a steep spatial gradient of amplitude over the array. Seizure onset was seen after a pre-ictal period marked by reduction in cone diameters and related evidence for large-scale disintegration that appeared to accompany or lead to loss of cortical metastability.

1. Introduction

Brain activity and functioning are characterized by a high degree of flexibility and robust stability of global state, which are reflected in both behavioral and the EEG. Behavioral evidence of brain flexibility comes from instantaneous changes in orientation and pursuit of goals in unexpected directions that are triggered by unpredictable conditions in the environment but that are controlled by neocortical activity. Behavioral evidence of brain stability is that each of these newly initiated behaviors is executed effectively, with rapid and reliable return of the brain to a state of readiness to respond to new contingencies. Electrophysiological evidence of brain flexibility come from the variety of spatiotemporal patterns of unit and dendritic activity that are related to behavior. Evidence for brain stability comes from demonstrations that reproducible patterns recur in reproducible behavioral states [Freeman, 2005]. Computational evidence for flexibility and stability comes from a hierarchy of models of nonlinear brain dynamics called K-sets [Freeman, 1975, 2000; Kozma and Freeman, 2001; Principe et al., 2001; Kozma, Freeman and Erdí, 2003], which are related to the models of Friston [2000], Tsuda [2001], and Stam et al. [2003], and which serve to simulate multiple states of unit and field potentials and their changes with learning. The multiplicity of states shows that brains are intrinsically unstable in jumping from each state to the next by state transitions, which closely resemble phase transitions in physical media [Haken, 1983]. Yet these multiple states collectively form a metastable collection of states of normal brain activity, each with its accompanying behavior. Epileptic seizures manifest a functional instability of brain by transitions to abnormal spatial and temporal patterns of unit and field potentials with abnormal behaviors, including partial complex seizures with *absence* [Freeman, 1986].

The focus of this report is on the spatiotemporal structures in the electroencephalographic (EEG) field potentials of the background activity in a human subject awake and at rest, in NREM sleep (behavioral sleep accompanied by large slow waves in the EEG and not with rapid eye movements), and preceding and during an epileptic seizure. This study was enabled by an opportunity to place a high-density array of electrodes onto the surface of the brain of a neurosurgical patient with medically intractable epilepsy, who was undergoing evaluation for possible surgical treatment. The work was based on prior studies in the nonlinear dynamics of neocortex in trained cats, rats and rabbits [Barrie, Freeman and Lenhart, 1996; Freeman, Gaál and Jornten, 2003] and gerbils [Ohl, Scheich and Freeman, 2001], in which intracranial EEGs were recorded during presentation of conditioned stimuli (CS). In those studies the animals were required to discriminate CS+ that were reinforced by reward or punishment from CS- that were unreinforced and subject to habituation. The dendritic potentials forming the EEGs were recorded with high-density electrode arrays giving windows on the surfaces of olfactory, visual, auditory and somatic primary receiving areas. This well-known "spontaneous" background EEG has been conventionally treated as "noise" and removed by averaging over multiple trials to derive event-related potentials that are postulated to signify cortical responses to impulse inputs like clicks, flashes, and so on. Avoiding time averaging enabled measurement of remarkable spatiotemporal structures in patterns of phase and amplitude in the background EEG [Freeman, 2004a,b, 2005]. The behaviorally related EEG patterns with CS were formed by phase transitions from the background attentive state to a state of categorizing the CS [Ohl, Scheich and Freeman, 2001; Ohl et al., 2003; Freeman,

2005], and their contents were mostly derived from pre-existing activity in the background relating to categories of stimuli and not from the stimulus-evoked activity. Yet despite the electrophysiological evidence for repeated phase transitions, whether or not induced by input, the sequences of brain patterns conformed to progressive and orderly movements in goal-directed behaviors, which demonstrated that the instabilities were encompassed in a higher degree of order comprising a 'metastable' state. Similar conclusions came from studies of unit activity by Fiseri, Chiuz and Welicki [2004] in visual cortex. These diverse studies support the inference that cortical instability embedded within a global metastable state is mandatory among the conditions for the flexibility of the brain in adapting to environmental changes.

The problem addressed in this report is how to describe the metastable state of the brain that can support the neocortical phase transitions that are required for rapid, reliable responses to environmental contingencies, as well as the breakdown in normal function that occurs leading to epileptic seizures. What are the neural mechanisms that make the brain and its EEG so robustly stable under a wide range of experimental conditions, and how might abnormal instability manifest itself in epilepsy? An approach to answering these questions has been devised by combining theoretical brain dynamics, neurosurgical practice, and new electrophysiological techniques for accessing fine spatiotemporal structures in EEGs using the Hilbert transform, by which very rapid changes in EEG can be measured. The temporal resolution given by the Fourier transform was restricted to intervals exceeding the wavelength of the frequency at which the phase was defined. The Hilbert transform gave the 'instantaneous' analytic phase, which tracked the time-varying frequency in aperiodic oscillations by measuring the broad-spectrum EEG in the subject awake and at rest, for which instability in metastability was normal, followed by studies of the subject asleep and then going into seizure. We interpreted our results on the basis of a dynamic model of partial complex seizure ('petit mal') in cortex [Freeman, 1986] that we attributed to loss of metastability. The signs of disorganization in the pre-ictal state might prove useful for systematic evaluation in clinical studies devoted to predicting seizures and explaining their causes.

2. Methods

2.1. Experimental subject and EEG recording

The subject was a 34 year old woman with a history of medically refractory complex partial seizures, who was a candidate for surgical therapy, who was monitored by EEG and video for eight days to record seizures. At the time that the clinical electrodes were placed, the attending neurosurgeon [GAW] with informed consent from the subject fixed an 8x8 channel, 10x10 mm microgrid onto the surface of the right inferior temporal gyrus. The monitoring time was dictated solely by clinical considerations, and there were no complications. The reference and ground placements for all 64 electrodes were respectively the Cz and Pz scalp locations (midline frontal and parietal sites in the standard 10-20 clinical system). The data were collected in the EEG and Clinical Neurophysiology laboratory of Harborview Hospital, University of Washington, Seattle, and sent by ftp without identifying personal information to the University of California at Berkeley for analysis. The data collection and management were governed by protocols approved by Institutional Review Boards in both institutions.

The data set used for the present review were selected in four segments approximately 2 minutes of recording with the subject in four states: awake and at rest; NREM sleep; performing a simple task (naming objects presented as visual images in a short term memory test); and during a typical seizure. The 8x8 array of stainless steel wires with interelectrode spacing of 1.25 mm gave an optimized spatial aperture of 10x10 mm [Freeman et al, 2000] that fit onto a single gyrus [Freeman et al., 2003]. The EEG was amplified with a Nicolet BMSI 5000 system having a fixed gain of 1628 and analog filters set at 0.5 Hz high pass and 120 Hz low pass. The ADC gave 12 bits with the least significant bit of 0.9 microvolts and maximal range of ±2,048*0.9 microvolts. DC offsets of the RC amplifier outputs were removed off-line by subtracting the channel means of every entire recording segment. Data were digitized at 420 Hz and down-sampled to 200 Hz. The amplitudes were normalized by dividing all 64 EEGs by the global standard deviation (GSD) of each segment.

2.2. Preprocessing EEG and calculating analytic phase and frequency

The Hilbert transform was used to get two essential quantities in each frame: the rate of change in phase with time (the frequency ω in rad/sec or Hz) and the rate of change in phase with distance (the gradient γ in rad/mm) [Freeman, 2004a]. Use of the Hilbert transform required further data preprocessing in four steps: (i) selecting 5 s blocks by visual editing; (ii) computing PSD_T (Fig. 2) and to find optimal filter settings; (iii) spatial low pass filtering with the cut-off at 0.2 c/mm at the concave upward inflection of the PSD_X (Fig. 4); and (iv) band pass temporal filtering at 12-30 Hz, 25-50 Hz or 12-55 Hz to extract the beta or low gamma range or both. The spatial PSD_X was the average of 1000 spectra over the 64 amplitudes at each time point. Higher spatial frequencies appeared to correspond mainly to the individual channel noise with relatively flat spectra. The temporal PSD_T was the average of the 64 spectra from 1000 data points. Both PSD were displayed in log-log coordinates. Further details are given in Appendices in Freeman [2004a,b].

The Hilbert transform was applied to the filtered EEG, v(t), to get the imaginary part, v'(t) [see Table 1.1 in Freeman, 2004a for a complete list of symbols]. The analytic amplitude was

given by the square root of the sums of squares of the real and imaginary parts. The analytic phase was given by the arctangent of the ratio of the imaginary part to the real part with base 2π ('atan2' in MATLAB). Details and rationales have been published previously [Freeman, Burke and Holmes, 2003; Freeman, 2005]. The phase measurements by the Hilbert transform were cross-validated by phase measurements using Fourier decomposition, within the limits of each method on temporal resolution [Freeman, 2004a].

The spatial gradient of phase was measured by using nonlinear regression at each window step to fit a cone in 2-D to the 8x8 phase values in the coordinates of the brain surface, either $\phi_{1,j}(t)$ from the Fourier method or $P_j(t)$ from the atan2 function by the Hilbert method. Four parameters were optimized in the equation for the cone, $\Phi(t)$, at each step with termination of iteration by minimization of least squares residuals:

$$\Phi_j(t) = \Phi_o(t) + \gamma(\square) ([x_j - x_o]^2 + [y_j - y_o]^2)^{.5}, \qquad j = 1, 64, \qquad (1)$$

where Φ_o was the offset of the vertical offset apex from the plane of fit, x_j , y_j gave the distance of the apex in mm from the center of the electrode array at x_o, y_o, and $\gamma(\square)$ was the slope of the cone in rad/mm in the t-th step of the window. Two passes were made with each phase matrix, one with the location of the phase maximum as the starting guess, the other with the phase minimum for initiation. The result was selected that had the least number of iterations to completion. On average convergence to solutions was achieved in >90-95% of windows with cones; failure to converge meant that no cone could be fitted. The % residuals for the phase cones was given by:

$$\% \text{ residual} = 1/64 \sum^{j} [\ \Phi_j(t) - \phi_{1,j}(t)]^2 \ / \sum^{j} [\phi_{1,j}(t)]^2, \qquad (2)$$

or $P_j(t)$ in place of $\phi_{1,j}(t)$. The values for $\gamma(t)$ and $\omega(t)$ were averaged:

$$\gamma_N = 1/n \sum^{n} \gamma\ (t_n), \qquad \omega_N = 1/n \sum^{n} \omega\ (t_n), \qquad (3)$$

where n was the number of time steps across which a stable phase cone had been defined. The frequencies, $\omega(t)$ and $f_1(t)$, were similarly averaged to get ω_N and f_N for the N-th cone.

2.3. Criteria for qualifying phase cones as stable; calculation of cone parameters

The Hilbert transform is notoriously difficult to apply to 1/f signals such as the EEG, owing to the high likelihood of introducing spurious 'phase slip'. The phase patterns from the analytic phase must be carefully screened by use of the following physiological criteria in order to separate phase slips from phase transitions [Freeman, 2004b], beginning with convergence to a solution with nonlinear regression that had to be achieved in >90-95% of time frames. This was also met in a large proportion of randomized controls, which illustrated that a phase cone could be fitted to many sets of random numbers, giving the appearance of structure where none might exist, or where spatial filtering imposed it. In order to exclude spurious phase structures from the analysis, supplemental anatomical and physiological evaluations were made of the acceptable parameter ranges: the location of the apex had to be within a distance twice the width of the array; the phase velocity had to be within the range of conduction velocities of cortical axons (1-10 m/s); the durations had to exceed 2 digitizing steps; and the half-power diameters could not exceed the width of the

cerebrum. These constraints were independently met by use of 5 computational criteria applied to the phase values from the Hilbert method, $p_j(t)$: (i) the locations of successive apices could not differ by more than the interelectrode distance (1.25 mm); (ii) the sign of the phase gradient of the cone, + or -, could not change; (iii) the SD_x of the analytic phase, AP, could not exceed 0.5 rad (iv) the SD_x of the analytic phase differences (CAPD) could not exceed 0.1 rad equivalent to 32 Hz in the 12-30 Hz pass band; and (v) the residuals from fitting a cone to the phase surface could not exceed 30%. Cones that met all of these constraints qualified as being stable. The criteria for stability of phase cones for the phase values from the Fourier method differed, in that (iii) and (iv) were replaced by the requirement that the residuals on the preliminary step of fitting the filtered EEG not exceed 20%. Statistical summaries of the distributions of the phase parameters in space and time were computed from the qualifying cones:

$$\text{Temporal wavelength, } W_t = 1000/(2\pi f_N) = 1000/\omega_N, \text{ ms/rad} \quad (4)$$

$$\text{Spatial length, } W_x = 1 / |\gamma_N|, \text{ mm/rad} \quad (5)$$

These parameters were approximately normally distributed. They were used to calculate physiological parameters of phase cones:

$$\text{Phase velocity, } \beta = W_x / W_t \quad \text{m/s} \quad (6)$$

$$\text{Diameter, } D_x = (\pi/2)\, W_x \quad \text{mm} \quad (7)$$

Controls by computing surrogate data, channel randomization, and shuffling have described in detail in a prior report on animal EEG [Freeman, 2004b].

3. Results

The identification of behavioral states was based on clinical evaluation of the 64 EEGs from the microgrid in the context of EEGs from the clinical array and the videotape of the subject at rest, engaged, in NREM sleep, or in seizure. The microgrid sampled 1 cm^2 from the approximate 1 m^2 of neocortex in a remote area of a diseased brain. Many seizures were electrographically restricted, involving only a subset of the clinical electrodes; those seizures were often distant from the array and did not involve it. Some seizures electrographically appeared to begin near the array because of high amplitude gradients but without clinical manifestations or even involvement of the larger clinical array. Electrographically local seizures appeared sporadically in states of otherwise behavioral wakefulness and sleep. Therefore, selected EEG epochs were assigned to the several states by evaluation of the context with the available information, but the selections could not be well controlled or guaranteed to be representative. However, the characteristics of the EEGs in the three groups and in the animal data served to outline a self-consistent description of the ranges of variation in dynamics among the several states.

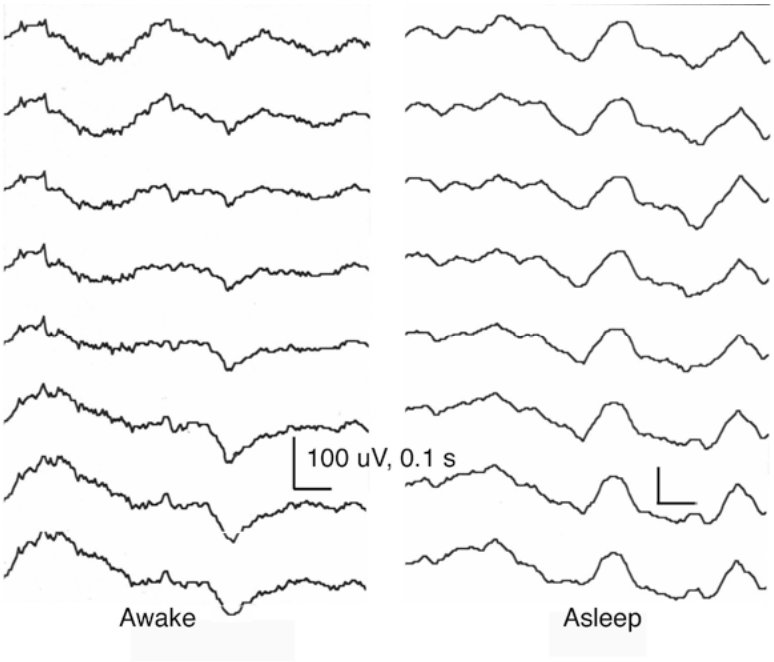

Fig. 1. A sample of 8 channels is shown from the 8x8 array implanted on the pial surface with spacing of 1.25 mm between electrodes. Small differences in the shared waveform among channels reveal a wealth of fine structure in the EEG.

3.1. Rate of change in PSD and phase gradients with the subject awake and asleep

On visual inspection the EEG signals from the 64 electrodes had very similar waveforms (Fig. 1) but with small differences in amplitude and phase that varied with the state of the subject (here comparing waking rest with NREM sleep). Because of the variability of these differences, the similarity of waveforms could not be ascribed to activity at the reference electrode in referential recording; thus the shared waveform could be described as a "carrier" wave subject to amplitude (AM) and phase (PM) modulation. The temporal PSD_T (Fig. 2)

displayed near-linear decrease in log power with increasing log frequency, "1/f" or in form f^{α}, where $\alpha \sim -2$ on average at rest and $\alpha \sim -3$ in sleep (Fig. 3).

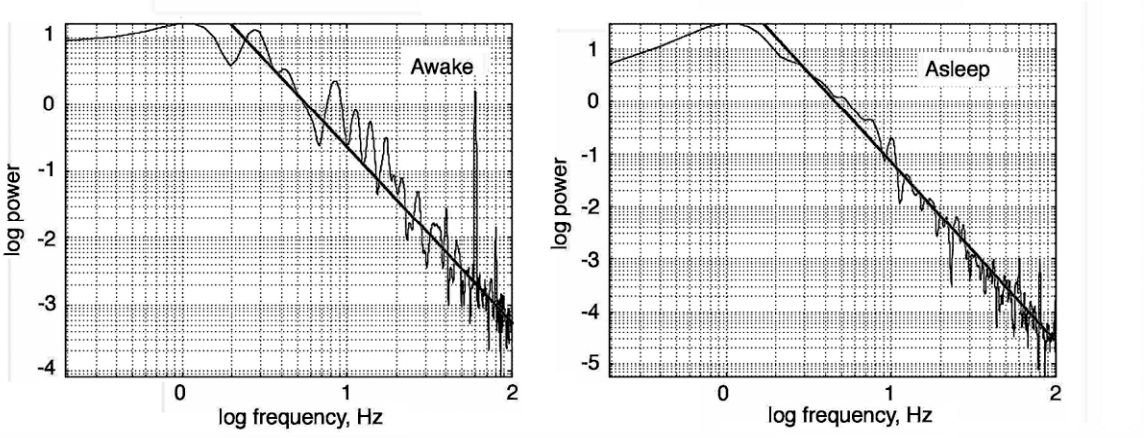

Fig. 2. The temporal power spectral densities (PSD_T) were calculated over epochs of 1000 digitizing steps (5 s) for each of the 64 channels and averaged across channels.

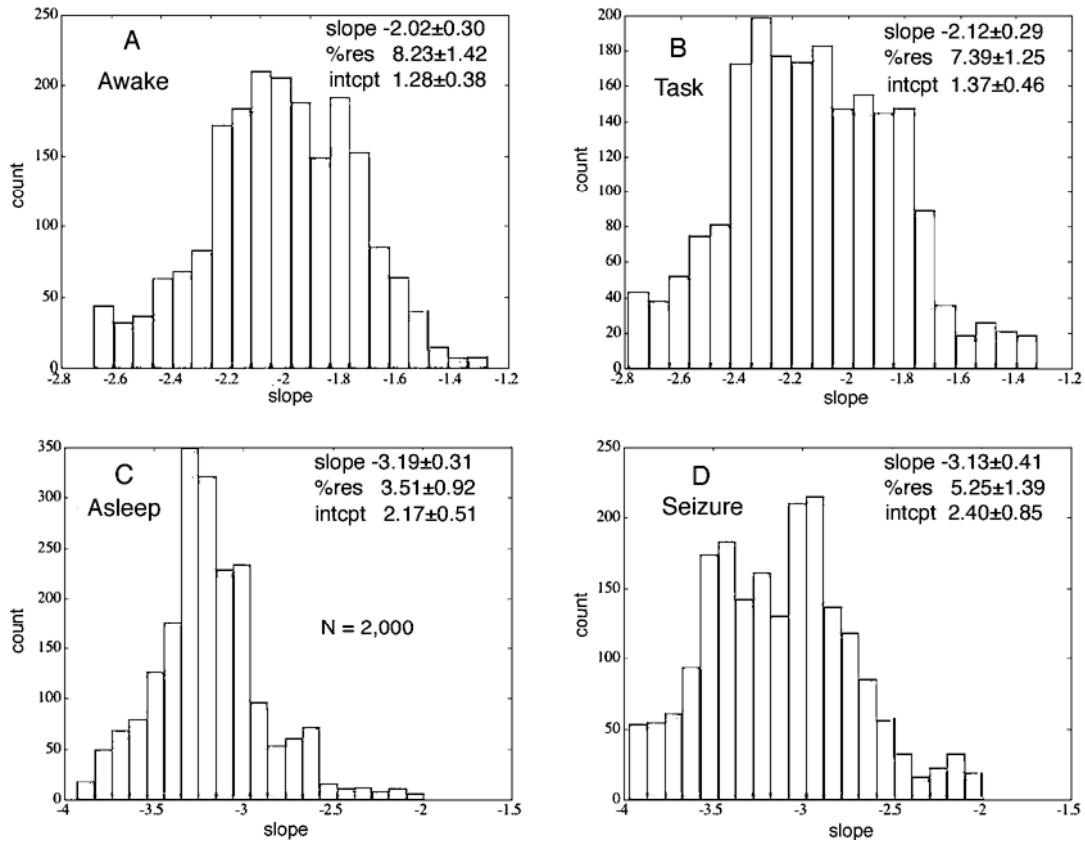

Fig. 3. A line was fitted to each of 2000 PSD_T to calculate the slopes, α, intercepts, and % residuals in four behavioral states.

The PSD_X from the three states were compared to those from rabbits (Fig. 4) in coordinates of log power vs. log normalized spatial frequency. The differences were numerically evaluated by an empirical "slope index" from calculating the difference in log power between the mean at the 5 highest frequencies and the mean at the 5 lowest frequencies. The

greatest differences were found in the sleep EEG. Lesser differences were found in samples from the wake EEG, but they seldom approached the small differences given by rabbit EEGs. In simulations of the PSD_X the values of the slope index decreased in relation to increasing measures of spatial coherence across the array.

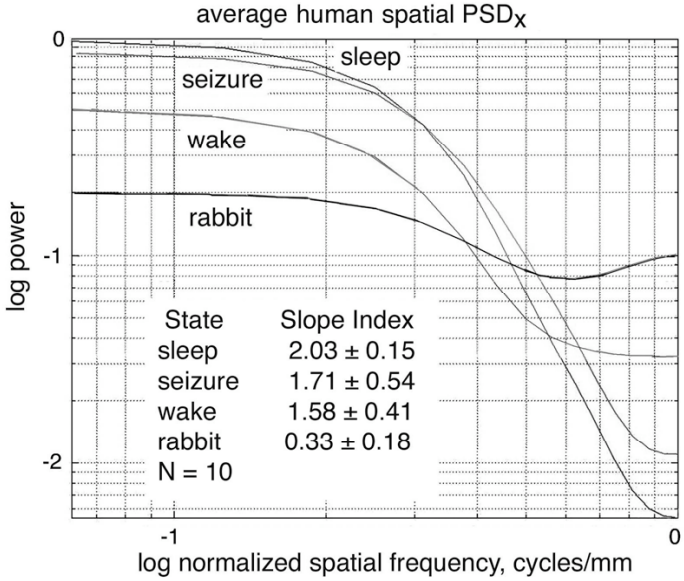

Fig. 4. Representative examples of PSD_X are compared in log-log coordinates. Normalization reduces the apparent power at low frequencies while enhancing it at high spatial frequencies. The increase in range of the normalized PSD_X from wake to seizure and sleep represents gain in power at of high spatial frequencies that we attribute to loss of long-range spatial coherence of underlying neocortical activity that sustains the EEG. Given the lack of an equation with which to fit the PSDX, an empirical "slope index" was calculated by the mean power in the lowest 5 spatial frequencies less the mean power in the highest 5 spatial frequencies in 25 PSD_X in ten 50 s records for each condition.

We restrict our presentation of phase data to the beta band (12-30 Hz) in order to simplify the description, because the phase structures in the gamma band were qualitatively similar to those in the beta band but less clear and less constant. Measurement of phase differences with respect to time (successive digitizing steps) and space (adjacent electrodes) gave access to two different phase structures. The temporal analytic phase differences from the Hilbert transform, $\Delta p_j(t)$, j = 1, 4, when displayed in a raster plot (Fig. 5), revealed sequences of plateaus of low phase differences corresponding to the mean frequency of the filtered EEG. Dips and spikes in phase differences (low and high instantaneous frequencies) tended to occur almost simultaneously on all channels, so we displayed the 8x8 signals in a single line for each time step. Alignment was designated as coordinated analytic phase differences (CAPD) [Freeman, Burke and Holmes, 2003].

The direction and magnitude of $\Delta p_j(t)$ varied widely, leading to high values of spatial standard deviation (SD_x) at the times of dips and jumps. The peaks in SD_x served as time markers for the CAPD. Superimposing plots of SD_x and the spatial average analytic amplitude at each time step showed that during the plateaus in SD_x in the awake state the amplitude increased across most of the durations of the plateaus (Fig. 6). The spatial SD_A of

the amplitude also increased with the mean amplitude, showing that epochs of high amplitude were spatially textured [Freeman, 2005].

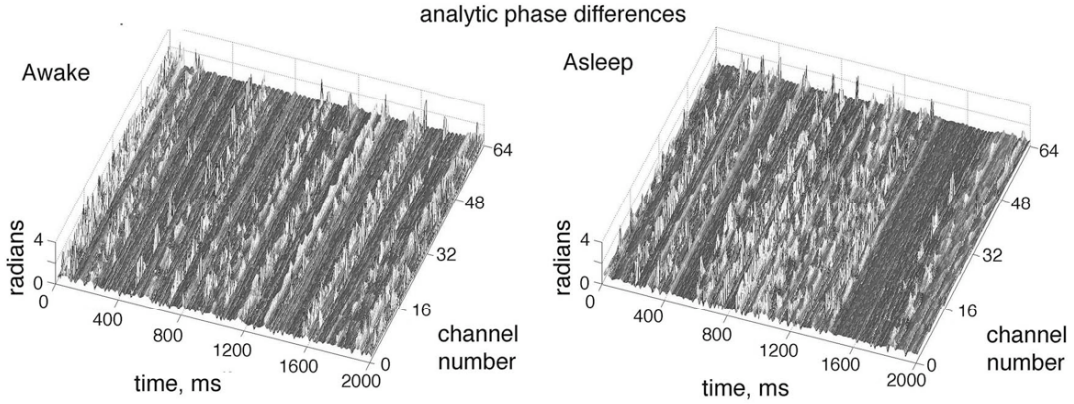

Fig. 5. Examples are shown of rasters of analytic phase differences, $\Delta p_j(t)$, j = 1, 64. This display aligned the 8 columns of the 8 rows along a single spatial dimension in order to demonstrate the coordination (CAPD) of the jumps and dips that bracketed the periods of low variation in phase. The temporal pass band was set at 12-30 Hz to cover the beta range.

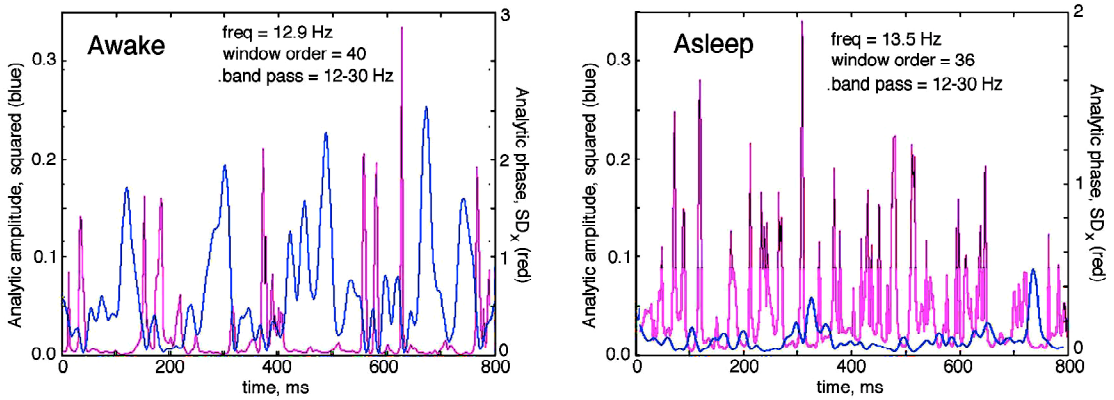

Fig. 6. The spatial standard deviation, SD_x, of $\Delta p_j(t)$ at each digitizing step demarcated phase transitions that bracketed phase plateaus that were accompanied by peaks in analytic amplitude in rest but not in sleep.

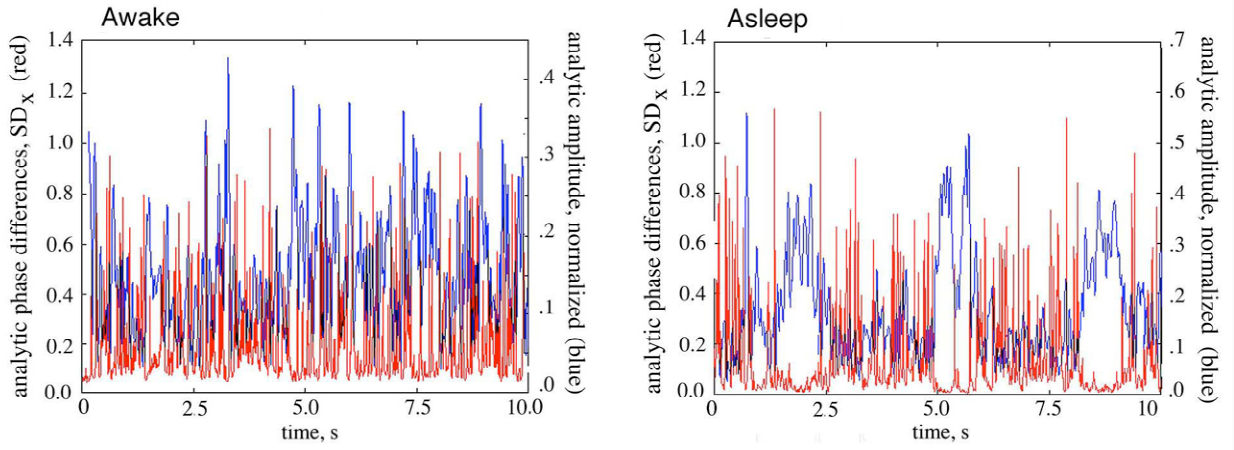

Fig. 7. The inverse relation of SD_x and analytic amplitude was sustained in rest with fluctuations in the theta range. In deep sleep the relation was replaced by intermittent prolonged 1 s epochs with absence of phase and amplitude patterns but high mean amplitudes.

The cospectrum of the crosscorrelation of SD_x and the unfiltered EEG over time periods of 10 s commonly showed a peak in the theta range (see Fig. 13, A below) in the rest state. Plateaus in SD_x also occurred in sleep but with shorter duration and without correlation with theta activity, as was commonly the case in the waking state [Freeman, Burke and Holmes, 2003]. The analytic amplitude remained low for most of the records in sleep and seldom peaked during the plateaus in SD_x. However, the extended time base of 10 s in NREM sleep revealed intermittent epochs at intervals of 2-4 s and lasting about 1 s (Fig. 7), in which SD_x remained low and the analytic amplitude rose to sustained high values, but the spatial SD_A did not, showing that despite the high mean amplitude, there was no spatial texturing; that is, there were no identifiable spatial patterns of amplitude detected in these 1 s epochs over the spectral range totaling 12-55 Hz. The range ≥60 Hz was not explored in the human data owing to artifacts.

In contrast to the absence of spatial amplitude patterns, the search for spatial patterns of phase revealed distinct phase structures. The application of the conic basis function to the 8x8 phase surfaces commonly yielded two or more overlapping phase cones, showing that phase values were co-varying in brief time periods at relatively constant rates in such a manner as to maintain constant frequencies at which orderly spatial structures of phase could form. Cone fits gave low residuals in phase plateaus but were not restricted to the plateaus, meaning that the widespread CAPD appeared to be superimposed on the phase cones. Short-lasting cones could be measured with phase from either the Hilbert and Fourier transforms, but the durations of cones lasting longer than one cycle of the carrier wave could only be estimated with the Fourier transform. Otherwise the mean values from the two methods did not differ significantly. Most qualifying phase cones persisted for durations commonly of 3 to 5 cycles of the carrier wave in states of rest (Fig. 8, A) and task performance but not in sleep.

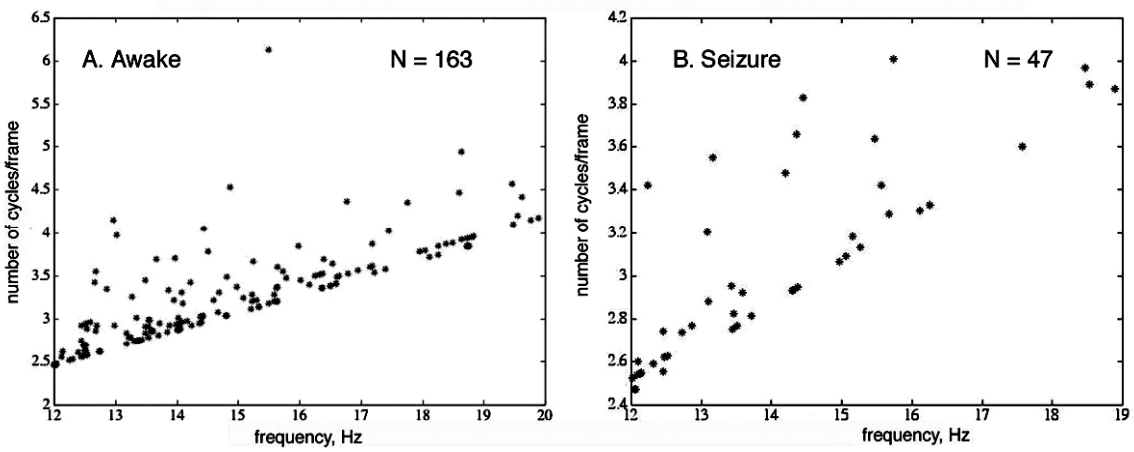

Fig. 8. The number of cycles in each qualifying phase cone in a 6 s time period is plotted against the carrier frequency. The oblique cut-off demarcated the width of the window in which the phase was measured, 0.2 s (40 bins).

There were no qualifying cones in the 1 s epochs. Examples of means and SD of the parameters of the cones from the Fourier method are listed in Table 1 for the pass band of 12-30 Hz and for a window of 200 ms (40 bins at the digitizing step of 5 ms). As shown in previous reports [Freeman et al., 2003; Freeman, 2004b] several of the parameters had power-law distributions (Fig. 9) both at rest (A) and in sleep (C), so that the values of the means and SD varied with the scaling of the measuring tools. As in all previous studies of phase cones, the locations and signs of the apices (maximal phase lead or lag) varied randomly from each qualifying phase cone to the next (Fig. 10) in both states though with fewer qualifying cones in sleep. Comparison of the awake and asleep states showed no significant differences in the means and SD of the cone measurements (carrier frequency and phase gradient) or in the derived quantities (cone diameter, phase velocity, and cone duration). EEGs were also recorded while the subject was engaged in a simple cognitive task of naming images of objects presented visually; no significant differences were found in either the temporal structures by CAPD or the spatial structures revealed by the conic basis function (Figs. 3, B; 8, B; 9, B; and Table 1).

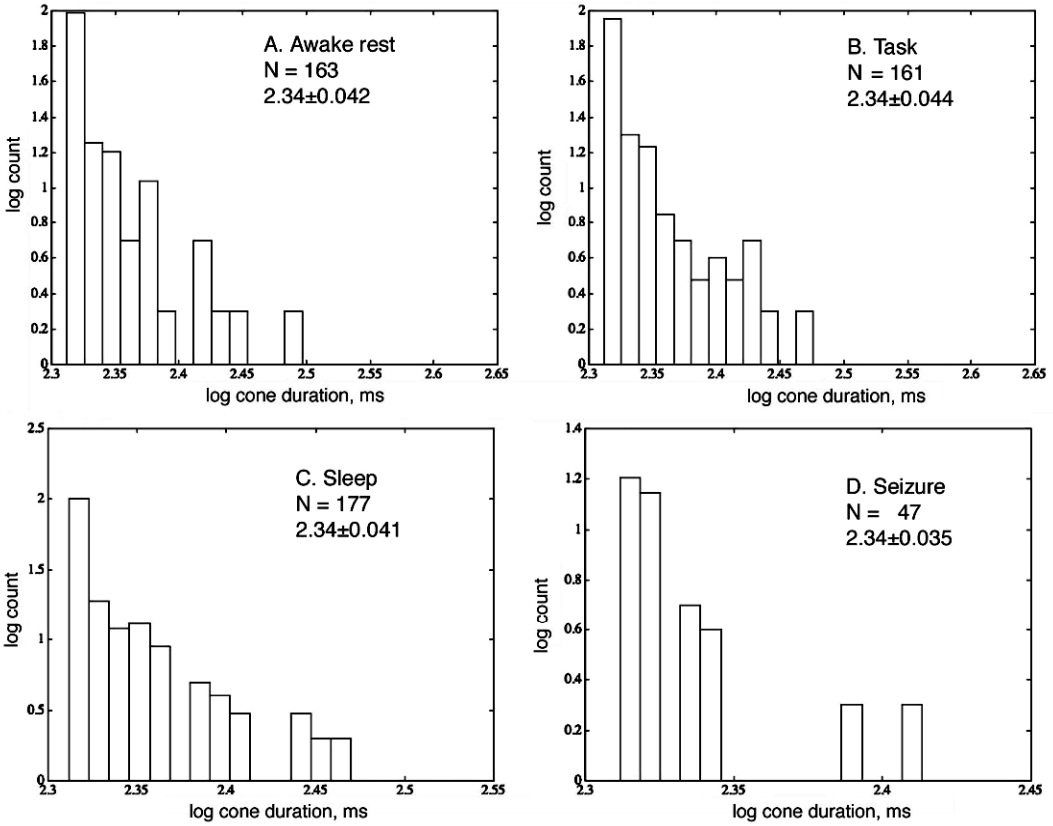

Fig. 9. The distributions are shown of cone durations in log-log coordinates to illustrate their power-law form. No minimal duration was found down to the digitizing step.

3.2. EEG phase gradients with the subject in transition to a seizure

The EEG records from this subject included multiple seizures for which neurosurgical intervention was warranted. An example in Fig. 11 compares representative EEG signals from the 3rd and 8th rows of the array in the pre-ictal rest state (A) 25 s before seizure onset

with the EEG signals taken 10 s into a seizure. The seizures were characterized by high amplitude waves at 3/s that were spatially distributed over a portion of the array (B), showing that the normal shared waveform (the carrier wave in the rest state (A) and the other three states was diminished or lost during the seizure. The PSD_T during seizure likewise often differed sharply from the 1/f form of the PSD_T in the rest and sleep states (Fig. 1) with high power in both the low and high theta ranges (D), corresponding to the 3/s wave that dominated the EEG.

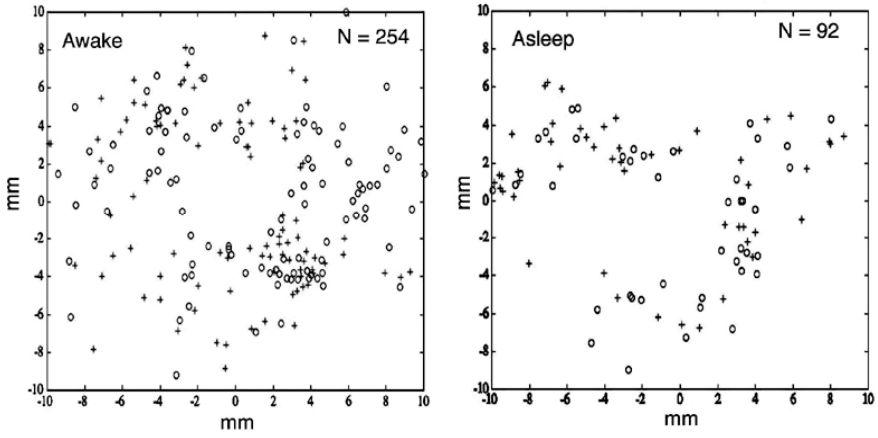

Fig. 10. The locations of the conic apices in 6 s at rest or in sleep are shown by (+) for phase lead and (o) for phase lag. The rectangle represents the 8x8 array. The absence of apices close to the center is unexplained. The center is where apices are expected when the phase cone is fitted to noise [Freeman, 2004b].

The distribution of the values of the slope, α, from fitting a line to the PSD_T was bimodal during the seizure (Fig. 3, D), in contrast to the unimodal distributions during the pre-ictal period and in the normal states. The raster plot of the analytic phase differences revealed diminished CAPD (Fig. 12, D). The cospectrum from the crosscorrelation of the SD_x from the analytic phase differences with the average unfiltered waveform of the EEG during the seizure (Fig. 13, D) showed the same peaks as in the autospectrum of the unfiltered EEG owing to the absence of peaks in the autospectrum of the SD_x. Phase cones were found during the seizure though relatively few in number. The most remarkable difference from the three normal states was the doubling of the phase gradient, which halved the estimates of phase velocity and cone diameter, and which further documented the loss of normal spatial integration of cortical activity implied by large phase cone diameters (Table 1). Although cone durations did not differ in the seizure state, the mean number of cycles/burst and the carrier frequency were reduced (Fig. 8, B). The sparse scatter of apices over the window resembled that in sleep (Fig. 10, D).

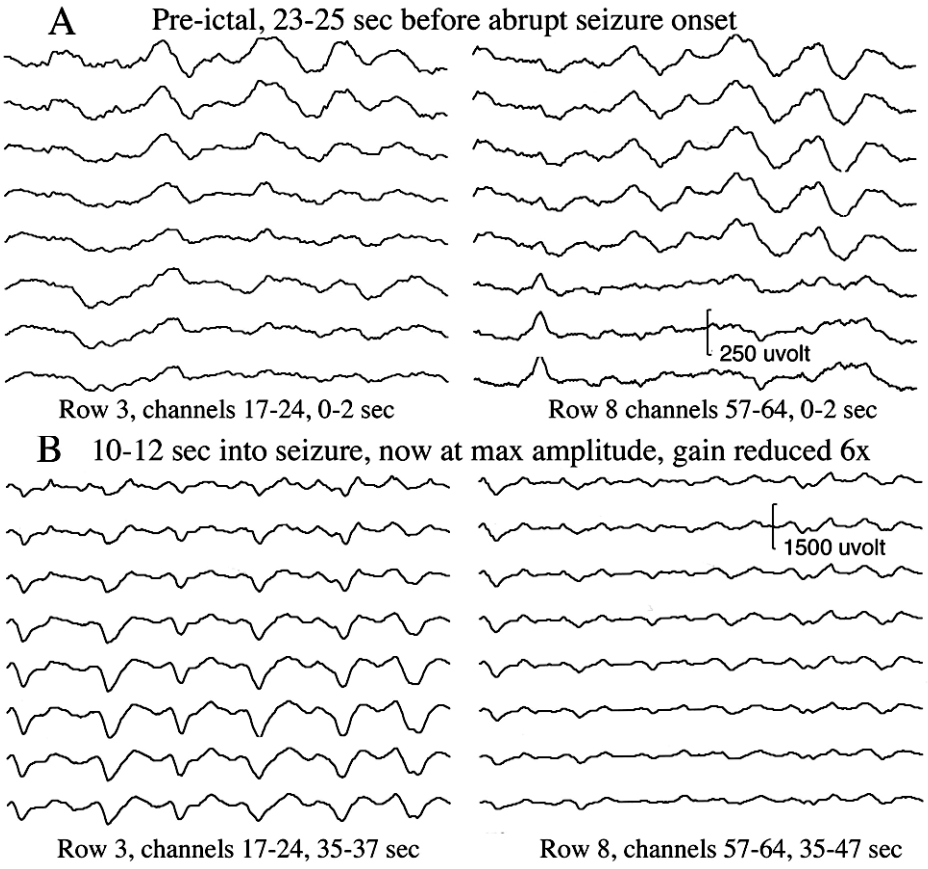

Fig. 11, A. A selection of eight representative channels in two rows illustrates the carrier wave and a normal amplitude distribution. **B.** The same channels during seizure reveal marked increase in amplitude unequally in the different parts of the array with unusually steep gradients.

Of further interest were changes observed in the half-minute preceding the seizure onset. The robust CAPD seen in the rest and task states diminished (Fig. 12, B) at 25 s and virtually disappeared (C) at 10 s. The proportion of the total variance incorporated by the first component of Principal Component Analysis (PCA) fell from normal values of 90-95% to under 70% (Table 2). The cospectra sampled 25 s and 10 s before the seizure onset showed (Fig. 13) that the small spectral peaks normally found in the theta, alpha and beta ranges (A) were diminished (B) or absent (C) as in sleep (Fig. 2). Yet the slopes of the PSD_T were not as steep as in sleep (Table 2). The inverse correlation between the plateaus in the CAPD and the peaks in the analytic amplitude found in the normal EEG (Fig. 14, A, B) disappeared, attesting to the diminished large-scale integration of the neocortical activity prior to seizure onset. The kind of large, sustained surge in amplitude shown in Fig. 14, C of a local seizure was never seen in normal EEGs, and it had no accompanying pattern of phase (D).

Table 1. Parameters of phase cones – Fourier method

Condition 12-30 Hz	N	frequency, f_i Hz	gradient, γ_k rad/mm	W_t ms/rad	W_x mm/rad
Awake	163	14.9±2.1	.072±.033	10.9±1.5	14.8±6.6
Asleep	177	13.8±2.0	.091±.055	11.7±1.3	12.6±6.2
Task	161	15.1±2/6	.089±.040	10.8±1.7	12.4±5.6
Seizure	47	14.0±1.9	.150±.073	11.6±1.4	5.3±8.6
Window 200 ms	rate 1/s	diameter mm	velocity, β m/s	distance mm	duration ms
Awake	3.3	24.9±7.7	1.51±0.56	7.7±4.0	219±25
Asleep	3.6	22.4±9.6	1.25±0.50	5.4±1.9	220±24
Task	3.2	20.7±8.0	1.26±0.55	5.7±1.8	220±25
Seizure	0.94	12.3±7.2	0.78±0.50	6.1±1.7	218±19

Table 2. Parameter shift from awake into seizure

Set	time s	gradient, γ_k rad/mm	velocity, β m/s	diameter mm
Awake	--	.070±.026	1.66±0.84	24.5±7.1
Pre-1	-25	.123±.048	0.87±0.36	14.9±6.1
Pre-2	-10	.150±.073	0.74±0.38	13.0±6.0
Seizure	+10	.141±.056	0.78±0.50	13.7±7.4
Set		exponent, α	intercept	%residuals
Awake		-2.12±0.29	1.37±0.46	7.39±1.25
Pre-1		-2.65±0.35	1.57±0.52	4.23±0.81
Pre-2		-2.72±0.31	1.62±0.42	4.17±0.93
Seizure		-3.12±0.41	2.40±0.85	5.24±1.39

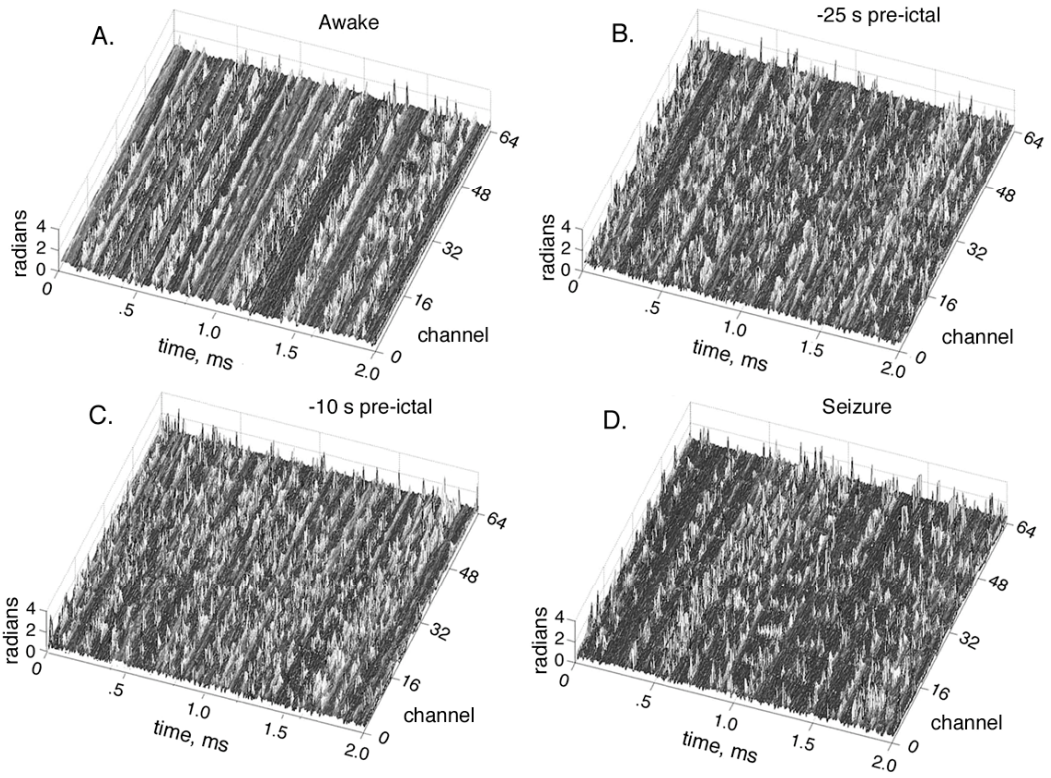

Fig. 12. Analytic phase differences as in Fig. 5 show loss of coordination (CAPD) before seizure.

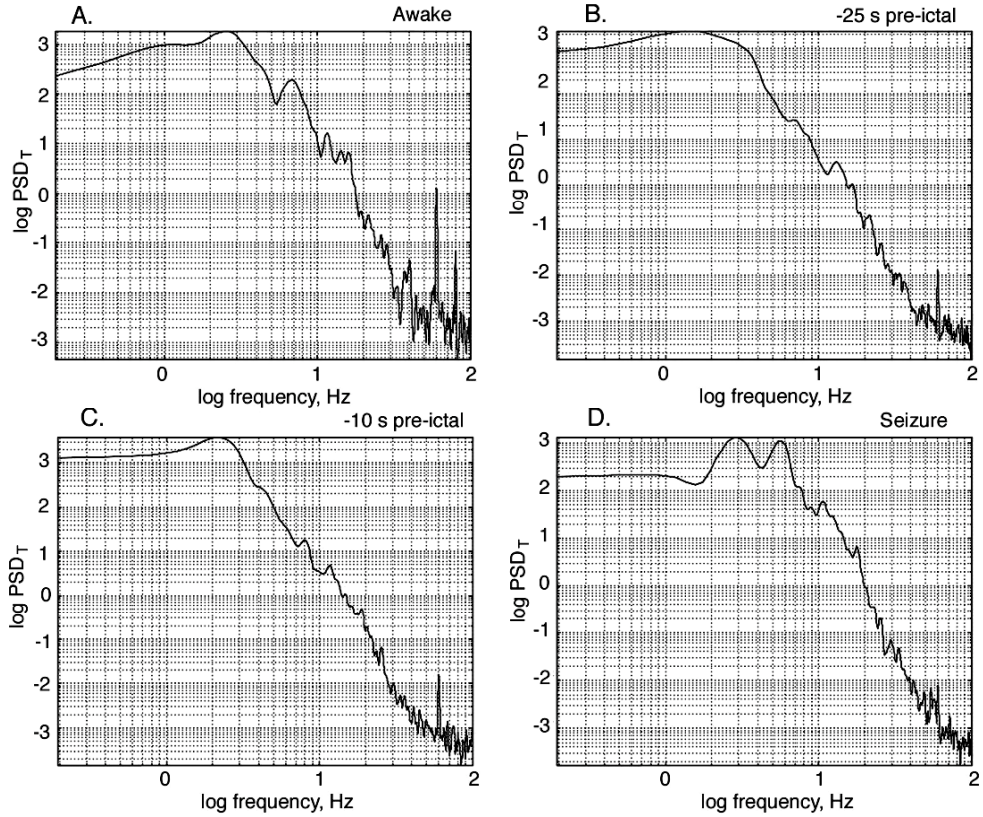

Fig. 13. Examples are shown of cospectra by the FFT of the crosscorrelation of the SD_x from the analytic phase differences in the beta range with the average of the 64 unfiltered EEGs.

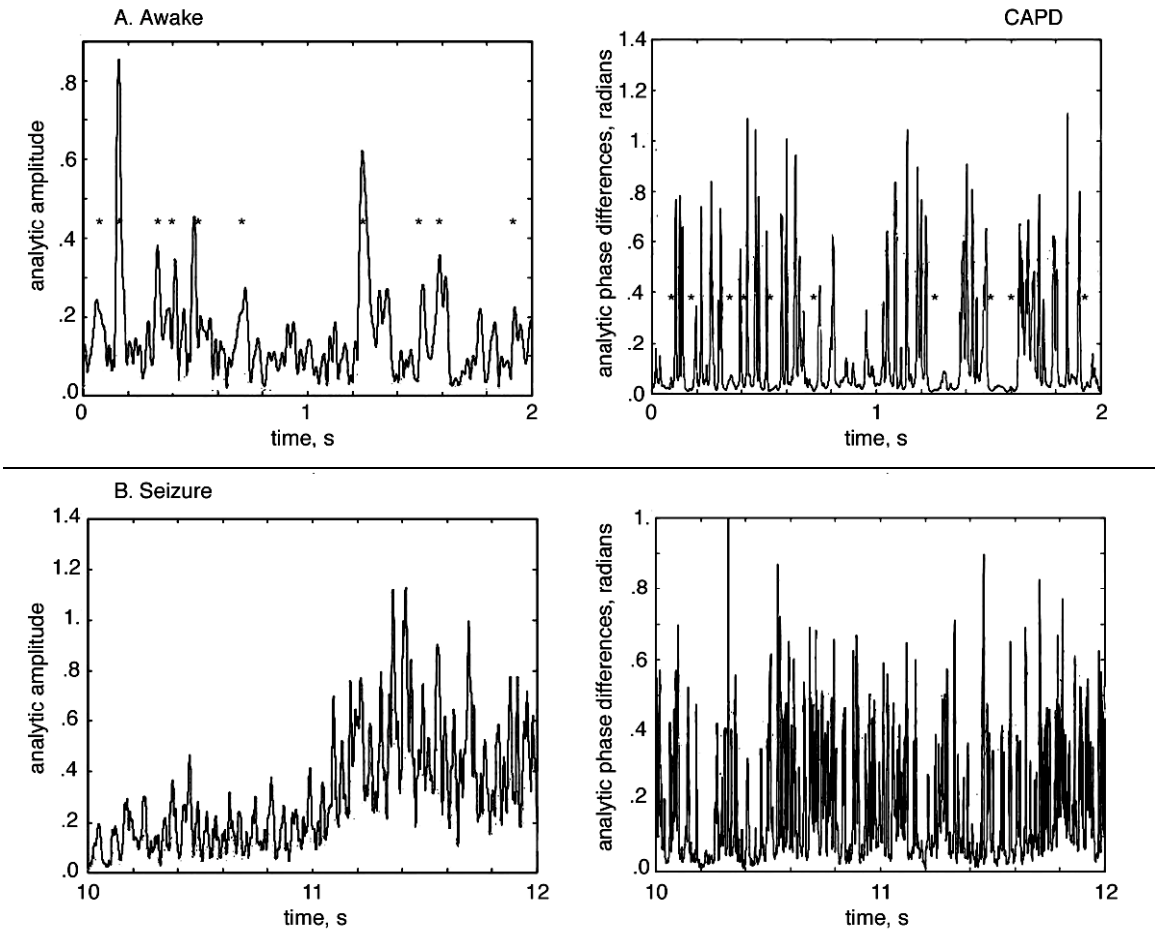

Fig. 14, A. The relation of the SD_x given by the CAPD to the mean analytic amplitude is shown in the state of awake rest and seizure. The asterixes in the left frame are aligned with the peaks in amplitude; the same asterixes in the right frame show the alignment with the low values of phase variance giving plateaus of stability. **B.** The peaks in amplitude and troughs in SD_x in the seizure state show no alignment.

4. **Discussion**

These data offer a first overview of complex spatiotemporal structures of phase and amplitude in multiple behavioral states of a human subject. The right inferior temporal gyrus was selected for the 1x1 cm window under surgical constraints, far from the sensory and motor areas of the brain and in a location known to be close to or in a diseased area of cortex, so the data are not directly applicable for modeling cognitive processes. Instead the data offer some insights into what we now conceive as a hierarchy of quasi-stable states in brain dynamics that may be useful in designing future experiments using high-density intracranial arrays and analyses of the data to test models of brain function. On the basis of present and previously published data we conceive the hierarchy in terms of the degree of spatiotemporal structure in the beta and gamma bands of the EEG or inversely the degree of symmetry [Breakspear and Friston, 2001]. The state of rest occupies a middle level and is characterized by prominent CAPD with peaks in analytic amplitude in the plateaus of low rate of change in

phase. We interpret the maximum in SD_x that precedes a plateau as evidence for the onset of a phase transition with four stages [Freeman, 2004a]: re-initialization of phase; re-synchronization of the oscillations in the plateau; re-stabilization of a spatial distribution of amplitude; and maximization of the energy of transmission of the stabilized distribution. The PSD_T in the rest state conforms roughly to 1/f having a slope near –2 (Fig. 3) in power spectra (α slope of –1 in amplitude spectra) with deviations in the form of peaks in the classical EEG ranges (Fig. 2). We postulate that multiple overlapping local cooperative domains form the ground state. Each domain has a carrier wave of dendritic currents with a phase cone and amplitude fluctuations whose sum with the dendritic currents of other domains creates the background EEG. Most of these cooperative states are quenched [Prigogine, 1980], but some of them provide the seeds for growth of amplitude patterns that emerge in the plateaus of phase stability. The durations, recurrence intervals, and apparently the diameters had power-law distributions, which along with the 1/f PSD_T and 1/f PSD_X indicated scale-free dynamics with self-similarity of spatial conic patterns.

We propose that the ground state in rest manifests a process of self-organized criticality [Jensen, 1998], in which the mean firing rates of neurons are held at a critical value throughout the cortex, homeostatically stabilized locally by their thresholds and refractory periods [Freeman, 2004b]. The grand average of the rates constitutes a global order parameter by which to designate that state quantitatively. The chaotic fluctuations in the beta and gamma range appear to manifest the response of the various areas of cortex to continuous bombardment by input from other areas and from subcortical nuclei. The bombardment induces local phase transitions that are reflected in the overlapping phase cones in neocortical EEG [Freeman, 2004b], most of which are small and short-lived, but some of which (under significant input) grow into major pattern shifts. The shared carrier wave then manifests the widespread synaptic interactions by which the spatial patterns are formed in phase transitions and maintained during phase plateaus. The increase in the spatial variance across the 64 amplitudes measured by SD_x indicates that the peaks in amplitude during plateaus are spatially textured, but the identification of the amplitude distributions as ‘spatial patterns’ can only be done at present in the sensory areas to which stimuli are directed [Freeman, 2005].

The onset of sleep is characterized by high amplitude slow waves and a shift in the PSD_T nearer to 1/f with a slope near –3 and loss of the peaks in the classical ranges. The phase cones persist along with the CAPD, but the peaks in amplitude no longer appear in relation to the plateaus (Fig. 6), so structure is lost, and symmetry is increased in this new state. In NREM sleep yet another state appears at irregular intervals, the prolonged 1 s plateaus, in which there is no evidence of CAPD, phase cones, or fluctuating distributions of amplitude, despite very large increases in mean amplitude. We propose that this intermittent state shows minimal structure and maximal symmetry, with a likely mechanism that synaptic bombardment from extracortical sources is briefly in abeyance. Two lines of investigation extend from this observation. On the one hand, Tononi and colleagues [Tononi and Cirelli, 2003; Huber et al, 2004; see also Hairston and Knight, 2004] hypothesize that the slowly recurring large scale waves are spatially accentuated in areas which were challenged during prior waking period, and that the network mechanisms underlying these slow waves may mediate synaptic down-scaling during sleep, thought to be required for increasing the signal-

to-noise ratio in the synaptic strengths and for maintaining stability in the face of widespread increases in synaptic strengths. They raise the question whether this process might not be global with local accentuation. There are striking spatio-temporal similarities between their large-scale waves in amplitude and our ensembles in phase. On the one hand perhaps the intermittent absence of spatial phase patterns observed in our study may reflect the time periods when cortex generates such slow, intrinsic mass activity that serves to scale the synaptic networks that were enhanced during the preceding period of waking. The return to the sustained sleep pattern constitutes symmetry breaking, and likewise the return to waking rest is yet another more complex symmetry breaking. On the other hand, Rosanova and Timofeev [2005], who studied the variations in responsiveness of somatosensory units to stimulation of median nerve vs. medial lemniscus during slow oscillations in sleep, noted that the frequency of recurrence of diminished responsiveness was on the order of 1/s. Perhaps the sporadic recurrence of the episodes of hyperstability in phase might better be interpreted as signs of impending but abortive instability leading to seizures, which were commonly observed during NREM sleep.

On the basis of studies in animals we proposed that the behavioral transition from waking rest to engagement with the environment is based in arousal that supports the likelihood of repetitive phase transitions recurring at rates in the theta range [Skarda and Freeman, 1987; Freeman, Burke and Holmes, 2003; Freeman, 2005]. Engagement would require a yet higher order symmetry breaking. However, owing to the location of the array far from sensory cortices, supporting evidence was not accessible. The striking difference in the spatial spectrum between rabbit and human (Fig. 4) may be evidence that the cortical area we observed in our human subject rarely, if ever, came into a state corresponding to full activation and engagement with behavior.

Lastly the seizure state was characterized by loss of the common waveform, bimodal distribution of values of α in $1/f^{\alpha}$, loss of the CAPD, loss of the inverse relation of low phase plateaus to high amplitudes, few phase cones, and unusually steep gradients of amplitude and of phase that coincided with reduced phase velocities and diameters of the phase cones. We attribute these properties to sustained loss of large-scale synaptic integration [Varela et al., 2001] that normally smoothes by cooperative interactions the local spatial variations in activity that arise through competitive inhibition and prevents breakdown of large-scale organization of neocortex [see also Chavez et al., 2004].

We infer that the mechanism of this pre-ictal state transition is a sustained increase in the activity of inhibitory interneurons in the cortex. Our inference is based on a study of partial complex seizures in the olfactory system [Freeman, 1986], in which unit recording disclosed a strong burst of firing by interneurons in Layer III during each 3/s wave, and depth recording showed that the wave was an IPSP generated by the pyramidal cells in Layer II. Simulation of the 3/s spike-and-wave train with the chaotic dynamics of the KIII set demonstrated that the seizure pattern resulted from runaway inhibition. The intense mutual inhibition can account for the loss of large-scale cooperation owing to enhancement of lateral inhibition. When interactions among inhibitory neurons rose to a high intensity with a deficit of excitation, an instability emerged in which by random fluctuations some neurons increased their activity, inhibited their neighbors, were disinhibited and thus more excited in

regenerative feedback that produced a self-limited explosive discharge of half the population and an IPSP in the excitatory neurons to which they projected. If this interpretation is correct, the use of GABA blockers would be indicated for treatment of this type of seizure.

In summary, three types of normal spontaneous symmetry breaking between four levels have been tentatively identified in EEG data: (i) from maximal symmetry in 1 s epochs in NREM sleep to maintained sleep with emergence of phase cones and CAPD without related peaks in amplitude; (ii) emergence of an inverse correlation between phase plateaus and peaks of amplitude; and (iii, in animal studies) emergence of CS-related spatial patterns in the amplitude peaks on engagement with the environment during perceptual discrimination. The seizure states are departures from this sequence into diminished global integration by sustained loss of long-range correlated activity, initially with loss of spectral peaks in the PSD_T, followed by explosive growth of local activity.

5. References

Barrie JM. Freeman WJ, Lenhart M. (1996) Modulation by discriminative training of spatial patterns of gamma EEG amplitude and phase in neocortex of rabbits. J Neurophysiol 76: 520-539.

Breakspear M, Friston K. (2001): Symmetries and itinerancy in nonlinear systems with many degrees of freedom. Behav Brain Sci 24: 813-814.

Chavez M, Le Van Quyen M, Navarro V, Baulac M, Martinerie J. (2003): Spatio-temporal dynamics prior to neocortical seizures: amplitude versus phase couplings. IEEE Trans Biomed Eng 50(5):571-83.

Fiseri, J, Chiuz C, Welikyi M (2004) Small modulation of ongoing cortical dynamics by sensory input during natural vision. Nature 431: 573-578; doi:10.1038/nature02907

Freeman WJ. (1975/2004) Mass Action in the Nervous System. New York: Academic Press; http://sulcus.berkeley.edu/MANSWWW/MANSWWW.html

Freeman WJ (1986) Petit mal seizure spikes in olfactory bulb and cortex caused by runaway inhibition after exhaustion of excitation. Brain Research Reviews 11:259-284.

Freeman WJ. (2000): Neurodynamics. An Exploration of Mesoscopic Brain Dynamics. London UK: Springer-Verlag.

Freeman WJ. (2004a) Origin, structure, and role of background EEG activity. Part 1. Phase. Clin. Neurophysiol. 115: 2077-2088.

Freeman WJ. (2004b) Origin, structure, and role of background EEG activity. Part 2. Amplitude. Clin. Neurophysiol. 115: 2089-2107.

Freeman WJ. (2005) Origin, structure, and role of background EEG activity. Part 3. Neural frame classification. Clin. Neurophysiol. In press.

Freeman WJ, Burke BC, Holmes MD. (2003): Aperiodic phase re-setting in scalp EEG of beta-gamma oscillations by state transitions at alpha-theta rates. Hum Brain Mapp 19:248-272.

Freeman WJ, Burke BC, Holmes MD, Vanhatalo S. (2003): Spatial spectra of scalp EEG and EMG from awake humans. Clin Neurophysiol 16:1055-1060.

Freeman WJ, Gaál G, Jornten R. (2003) A neurobiological theory of meaning in perception. Part 3. Multiple cortical areas synchronize without loss of local autonomy. Int J Bifurc Chaos 13: 2845-2856.

Freeman WJ, Rogers LJ, Holmes MD, Silbergeld DL. (2000): Spatial spectral analysis of human electrocorticograms including the alpha and gamma bands. J Neurosci Meth 95:111-121.

Friston KJ. (2000): The labile brain. I. Neuronal transients and nonlinear coupling. Phil Trans R Soc Lond B 355:215-236.

Haken, H. (1983): Synergetics: An Introduction. Berlin: Springer-Verlag.

Hairston IS, Knight RT (2004) Sleep on it. Nature 430: 27-28.

Huber R, Ghilardi MF, Massimini M, Tononi G (2004) Local sleep and learning. Nature 430: a78-81.

Jensen HJ. (1998): Self-Organized Criticality: Emergent Complex Behavior in Physical and Biological Systems. New York: Cambridge UP.

Kozma R, Freeman WJ (2001): Chaotic resonance: Methods and applications for robust classification of noisy and variable patterns. Int J Bifurc Chaos 10: 2307-2322.

Kozma R, Freeman WJ, Erdí P (2003): The KIV model – nonlinear spatio-temporal dynamics of the primordial vertebrate forebrain. Neurocomputing 52:819-826.

Ohl FW, Scheich H, Freeman WJ. (2001): Change in pattern of ongoing cortical activity with auditory category learning. Nature 412:733-736.

Ohl FW, Deliano M, Scheich H, Freeman WJ (2003) Early and late patterns of stimulus-related activity in auditory cortex of trained animals. Biol. Cybernetics 88: 374-379.

Prigogine I. From Being to Becoming: Time and Complexity in the Physical Sciences. WH Freeman, San Francisco, 1980.

Rosanova M, Timofeev I (2005): Neuronal mechanisms mediating the variability of somatosensory evoked potentials during sleep oscillations in cats. J. Physiol. 562: 569-582.

Skarda CA, Freeman WJ (1987): How brains make chaos in order to make sense of the world. Behavioral and Brain Sciences 10: 161-195.

Stam CJ, Breakspear M, van Cappellen van Walsum A-M, van Dijk BW. (2003): Nonlinear synchronization in EEG and whole-head recordings of healthy subjects. Hum Brain Mapp 19: 63-78.

Tononi G, Cirelli C (2003): Sleep and synaptic homeostasis: a hypothesis. Brain Res Bull 62: 143-150.

Tsuda I. (2001): Towards an interpretation of dynamic neural activity in terms of chaotic dynamical systems. Behav Brain Sci 24:793-810.

Varela F, Lachaux J-P, Rodriguez E, Martinerie J. (2001): The brain-web: phase synchronization and large-scale integration. Nature Rev Neurosci 2:229-239.